Research Square

Preprints are preliminary reports that have not undergone peer review.
They should not be considered conclusive, used to inform clinical practice,
or referenced by the media as validated information.

A novel, rapid culture-free method for the identification of twenty UTI-causing bacterial species directly in urine

Srijan Jindal

Srijan.jindal@innotivedx.com

Innotive Diagnostics

Kate James

Innotive Diagnostics

Dolores Nicoletti

Innotive Diagnostics

Megan Victoria Jackson

Innotive Diagnostics

Andrew David Sails

Innotive Diagnostics

Alexandre Seewald-Butzerin

Innotive Diagnostics

Daniel Hughes

Innotive Diagnostics

James Roberts

Innotive Diagnostics

Anna Barbano

Innotive Diagnostics

Article

Keywords:

Posted Date: September 22nd, 2026

DOI: https://doi.org/10.21203/rs.3.rs-11084926/v1

License: This work is licensed under a Creative Commons Attribution 4.0 International License.
Read Full License

Additional Declarations: Competing interest reported. This study was funded by Innotive Diagnostics. All authors are employees of Innotive Diagnostics. The technology described in this paper is the subject of two patent applications filed by Innotive Diagnostics Limited (European (EP) Patent Application No: 26170637.8 and U.S. Patent Application No. US20250052744A1).

Abstract

Conventional urine culture requires 24–48 hours for pathogen identification and antimicrobial susceptibility testing (AST), delaying targeted therapy for urinary tract infections (UTIs) and worsening antimicrobial resistance. A rapid, accurate, and culture-free point-of-care diagnostic test is required to accurately diagnose UTI and guide the selection of effective antibiotic therapy. Here, we present a novel culture-free method for identifying bacteria directly from urine specimens using high-resolution transillumination alongside multiplexed fluorescence microscopy. This method creates a unique Multi-Parametric Signature for target bacteria by capturing both fluorescence data from a four-dye panel and morphological features. A Histogram Gradient Boosting (HGB) classifier, trained on 191 strains, successfully identified 20 uropathogenic bacterial species with an accuracy of 99.3%. The complete process from sample to identification can be achieved in under 15 minutes in an automated commercially viable setup and is compatible with workflows incorporating enumeration and downstream AST. Compared to conventional culture, MALDI-TOF, and genotypic testing, this technique combines operational simplicity, speed, cost-effectiveness and the ability to rapidly expand the panel. This innovative method sets a new gold standard for identification of bacterial uropathogens, providing rapid, precise species-level identification to support improved clinical outcomes.

Introduction

The antimicrobial resistance (AMR) crisis is estimated to kill over 10 million people annually by 2050, with approximately 8.22 million deaths predicted to be associated with, and 1.91 million attributed to, AMR [1,2]. In 2021, about 4.71 million deaths were associated with AMR, and 1.14 million were attributed to AMR [1]. It is widely acknowledged that urgent action is necessary to prevent widespread human suffering and global economic damage [3]. Inappropriate prescribing[4–7] and the overuse of antibiotics[8–10] in primary and secondary care settings are among the leading drivers of AMR. Hence, it is critical to prescribe the correct antibiotic upon the patient's initial clinical encounter [11,12]. For accurate prescribing of effective antibiotic therapy to occur, rapid, cost-effective, and accurate point-of-care diagnostics are required.

There are over 400 million cases of Urinary Tract Infections (UTIs) worldwide annually [13] which are responsible for approximately 22.7% of all the antibiotic prescriptions in England [14]. Some studies [15,16] suggest that about 50–70% of all UTI-related antibiotic prescriptions may be wrong or unnecessary, making UTIs one of the leading infections for which antibiotics are misprescribed [17,18]. UTIs are one of the most common bacterial infections found in both community and hospital settings, posing a huge clinical and economic burden on global healthcare systems [9,19,20]. It is estimated that 50–60% of adult women will experience at least one UTI in their lifetime, making it the most common bacterial infection for this group [21].

The scale of the problem places a significant strain upon healthcare resources, with UTIs being one of the leading causes of emergency hospital attendance and admission [22]. The economic impact is substantial, with hospitalisation costs for complicated UTIs (cUTIs) in the US ranging from approximately $9,400[23] to over $32,000 for catheter-associated UTIs (CAUTIs) in paediatric populations [24]. These costs escalate dramatically if multidrug-resistant (MDR) pathogens are present, where treatment becomes more complex and prolonged [19]. In the US alone, the cost of treating patients hospitalised due to UTI is estimated at around $45 billion annually[25]. If treated incorrectly, UTIs can lead to severe life-threatening diseases, including pyelonephritis, bacteraemia and sepsis, emphasising the critical need for accurate and fast diagnostic tools [20,26,27].

The gold-standard diagnosis of UTI relies upon conventional microbiological culture of the urine sample [28,29]. This method involves inoculating a known volume of urine on a culture plate and incubating it for 18–24 hours, after which time bacterial colonies may be observed [30]. The presence of infection is determined by counting the number of bacterial colonies, calculating the bacterial concentration in the original sample and comparing this value to an established threshold to determine if the patient has a UTI. The use of specific selective UTI agar media can be used to identify the bacterial species/genus at the same time [31]. If the sample is considered to be positive for UTI, an antibiotic susceptibility test may be performed, which takes another 18–24 hours [28,32]. The total turnaround time (TAT) from sample collection to a correct actionable prescription is 48–72 hours, which includes transportation, handling, and storage of the samples. Although microbiological culture provides comprehensive phenotypic data, its delayed TAT means clinicians treat patients with empirical antibiotics, which increases the burden of antimicrobial resistance [33,34]. Beyond the slow TAT, the diagnostic accuracy of this method is often compromised by poor specimen handling, substandard transportation and improper storage of the clinical sample prior to testing, and cross-contamination during sample processing [34,35]. Furthermore, the improper use of broad-spectrum antibiotics accelerates the development of multidrug-resistant organisms [36]. The presence of antibiotic resistant organisms result in longer hospital stays, treatment failures and death, resulting in higher healthcare costs and an increase in the burden of antimicrobial resistance [19,37].

Due to the delayed turnaround time for conventional microbiology culture results, clinicians typically rely on clinical symptoms and point-of-care (POC) urine dipstick tests for immediate clinical decision making [38–40]. The low accuracy of dipsticks has been widely reported. Sensitivity and specificity vary considerably between studies, with reported sensitivities ranging from 62.7% to 90.0% and specificities from 39.0% to 73.9% [41,42]. Furthermore, specificity may decrease to as low as 39.0% in older patients[43].

Recent years have seen an emergence of rapid diagnostic tests for UTIs [44–47]. For such tests to support appropriate antibiotic prescribing, three functions are broadly required: detection of infection/pathogen enumeration, bacterial identification and AST. 216Dx UTI [48,49], Uriscreen [50,51], Jimini [52], UTI-lizer [53] and UTRIPlex [50] are some of the technologies aimed at providing rapid detection directly from urine. Various

commercial [54,55] and in-development [56–64] rapid AST technologies exist, and while these may provide useful susceptibility data, their clinical value could be further enhanced by pairing with rapid bacterial identification to assist clinicians in selecting appropriate antibiotics.

Despite this progress, rapid bacterial identification for UTIs remains an area of considerable unmet need, with only a few technologies in development. A recently developed 40-minute test uses loop-mediated isothermal amplification (LAMP) to amplify and detect DNA from target bacteria. This method achieves 86.1% accuracy, but is limited to a panel of six bacterial groups and is unable to distinguish between live and dead cells [65]. Another technology uses microfluidics to manage and monitor single-cell metabolic responses, however, a four-hour turnaround time may limit its applicability outside its current proposed centralised laboratory settings [66]. A technology reported using fluorescence in-situ hybridisation (FISH) and magnetic particles to identify bacterial species in approximately 45 minutes and an AST result in around five hours [58] and further technology described uses a surface affinity binding approach utilising glycan-coated fluorescent particles for identifying specific bacterial species [67]. Collectively, while these technologies represent progress towards rapid UTI diagnostics, none fully provide accurate, species-level bacterial identification for a comprehensive panel of species within a clinically useful timeframe, a gap that the present work aims to address.

The UTI point-of-care diagnostics market is undergoing a much-needed fundamental transformation, moving toward rapid testing. The existing diagnostic solutions reveal a critical gap, i.e., the need for a point-of-care technology that combines speed, accuracy and clinically actionable phenotypic information. We describe a novel and rapid culture-free method that bridges this gap, combining high-resolution microscopy with multiplexed fluorescent dyes to generate a bacterial Multi-Parametric Signature (MPS) directly from urine. Our novel method stains the live cells with fluorescent dyes without compromising the cell membrane. Subsequent incubation and imaging of the cells using high-resolution fluorescence microscopy and use of a pre-trained algorithm enables the species to be identified. This multiparametric, phenotypic approach provides an accurate, species-level identification of bacterial cells direct within urine in under 15 minutes. We demonstrate accurate identification of 20 UTI-related bacterial species using this method. By delivering rapid pathogen identification, this technology equips clinicians with early insights to guide initial patient management. Furthermore, Innotive Diagnostics is actively developing integrated enumeration and AST capabilities which will integrate with this rapid identification, ultimately enabling a comprehensive diagnosis and accurate antimicrobial susceptibility result in a point-of-care solution.

Methods

Bacterial Strains and Culture Conditions

One-hundred and ninety-one uropathogenic bacterial isolates were used in this study (Supplementary Table S1). All bacterial isolates were identified to the species level using MALDI-TOF mass spectrometry.

For long-term storage, strains were stored at -80°C in a 25% (v/v) Glycerol (Fisher Scientific) solution in Tryptic Soy Broth (TSB; VWR). Frozen bacterial stocks were recovered by streaking them onto Mueller Hinton Agar (MHA; Oxoid) and incubating at 37°C for 18-48 hours depending on the species, until distinct single colonies were observed.

Preparation of Bacterial Suspension in Urine

Strains were grown in 0.22 µm-filtered Drug-Free Pooled Human Urine (2B Scientific) at 37°C as shown in Figure 1. Incubation times and shaking conditions varied by species to achieve exponential phase growth; refer to Supplementary Table S2 for conditions used for each species.

Multiplex Fluorescent Staining and Sample Preparation

Bacterial cultures were adjusted to approximately $1x10^7$ cells/mL using a sterile-filtered, bacteria-free urine matrix in which the the cells were grown. Stock concentrations of four fluorescent dyes, SYTO 13 Green Fluorescent Nucleic Acid Stain, 3,3'-Dipropylthiadicarbocyanine iodide (DiSC3(5)), SYBR Green I nucleic acid gel stain and N-(3-triethylammoniumpropyl)-4-(6-(4-(diethylamino)phenyl)hexatrienyl)pyridinium dibromide (FM 4-64) (all from Fisher Scientific) were prepared according to manufacturer's recommendations.

Three separate 1 mL bacterial aliquots of ~$1x10^7$ cells/mL were prepared. The first aliquot was stained with SYBR Green I (10x) and $DiSC_3(5)$ (3 µM). This was done because the fluorescence spectra of these two dyes do not overlap and they stain different parts of the bacterial cells. The second and the third aliquots were stained with SYTO 13 (3 µM) and FM4-64 (15 µM), respectively.

Fluorescence Microscopy and Image Acquisition

Dried agarose pads were prepared on microscope slides and were placed onto an EVOS M7000 microscope (Invitrogen) with an on-stage incubator (Invitrogen) which was pre-warmed to 37°C. Twenty-five microlitres of each bacterial aliquot plus dyes were inoculated onto separate agarose pads and allowed to rehydrate the pads for 10 minutes. A square of breathable film (eMagTech) was placed over each pad. Images were acquired under 40x magnification.

The specimens containing the dyes SYBR Green 1, SYTO 13, and DiSC3(5) were all imaged at an intensity of 0.0002. An EVOS Light Cube, GFP (Invitrogen) was used for SYBR Green 1 and SYTO 13, and an EVOS Light Cube, Cy5 2.0 (Invitrogen) was used for DiSC3(5). The specimens containing the dye FM 4-64 were imaged with an EVOS Light Cube, RFP 2.0 (Invitrogen) at an intensity of 0.005. Transillumination images used white light at an intensity of 0.0065. Ten images illuminated using transillumination and

fluorescence were captured for every dye, totalling 40 transillumination images and 40 fluorescent images per sample.

Algorithm and Image Processing

The image processing pipeline converted raw microscope images into structured fluorescence and morphological data through a sequence of segmentation, normalisation, and feature extraction steps.

Transillumination images were used to perform geometric analyses, extract cellular morphology statistics and generate a precise cellular segmentation model. A segmentation model, based on a convolutional autoencoder with encoder-decoder architecture, was applied to transillumination images to classify every pixel as either microorganism containing or background, generating a binary mask for each image. These masks were aligned and applied directly to their corresponding fluorescent illumination images to delineate individual bacterial cell regions. This ensured that only pixels containing actual cells, rather than imaging artefacts or out-of-focus features, were used for downstream analysis. A background subtraction algorithm was then applied to each fluorescence image to remove background signal. A per-pixel measurement produced characteristic intensity histograms for each fluorescence channel.

Baseline cell morphology (cell shape and size, derived from axis analysis of segmented regions) was extracted from the transillumination images using a bespoke algorithm combined with a shape predictor.

For each detected microorganism region, a per-pixel measurement step captured raw pixel intensities and normalised them to a fractional scale from 0 to 1, making the data independent of image bit-depth and compatible across imaging sessions. Histograms were computed by counting the number of pixels falling within each predetermined intensity range, producing a frequency distribution for every fluorescence channel and every cell region.

In addition to global per-image histograms resolved at the image level, orientation normalised morphological and texture descriptors were extracted from individual bacterial cells across all channels, such as co-occurrence texture coefficient of variation (roughness, measured through a Gray-Level Co-occurrence Matrix), longitudinal polar staining and orientation-normalised cell shape structures.

Data Analysis

The computational framework for bacterial identification comprised a sequence of feature extraction, Multi-Parametric Signature (MPS) generation, and classification.

The feature extraction pipeline processed the outputs above for 34,184 transillumination and fluorescence illumination images. For each sample, the system generated a signature by combining three feature families: (i) pixel intensity histograms for every imaging channel with relevant bacterial strain metadata; (ii) single-cell resolved morphological and texture descriptors across all four fluorescence channels; and (iii) population-level heterogeneity indices computed as the coefficient of variation (standard deviation normalised by the mean) for each morphological and intensity invariant parameter. This captures the cell population characteristics of specific species.

To prepare the data for classification, a series of statistical normalisation steps were performed, and additional descriptive distribution statistics were calculated to capture the underlying morphology and distribution of the data.

A Multi-Parametric Signature was generated by aggregating the cellular morphology metrics and the fluorescence histograms into a single high-dimensional feature vector. As these vectors combine the spectral data from all four dye channels with those morphology metrics, they act as a unique biometric signature for each sample.

For visual inspection and quality control, pixel intensity histograms were rendered as heatmaps (Figure 6) with fluorescence intensity on the x-axis and coverage (percentage of cells) on the y-axis, producing composite species spectra that enabled rapid identification of inter-species differences in dye uptake patterns.

Classification was performed using a histogram gradient boosting (HGB) classifier, an ensemble technique that builds predictive models sequentially using multiple decision trees to minimise residual errors from preceding stages. A training matrix was constructed from the component image feature vectors and subsequently divided into training and test sets at a 4:1 ratio, stratified by species to ensure balanced representation. The training set was used by the classifier to create a model which was then able to generate predictions against the test set.

Results

Input dataset

A total of 191 uropathogenic bacterial isolates spanning 20 species were included in this study, encompassing common community-acquired uropathogens alongside species frequently associated with nosocomial and complicated urinary tract infections. The complete species panel is summarised in Supplementary Table S1.

For each isolate, up to 10 image sets were acquired per dye combination, with parallel capture of multi-channel fluorescence and transillumination images from the same field of view. Each image set comprised four fluorescence channels, DiSC3(5), SYBR Green I, SYTO 13 and FM 4-64, paired with a

corresponding transillumination image of the identical specimen location (Figure 2). These raw, paired optical datasets served as the primary input for downstream multi-parametric analysis.

Segmentation accuracy

Transillumination images were processed to isolate individual bacterial cells and remove imaging artefacts (Figure 3). A pre-trained convolutional neural network generated binary segmentation masks identifying cell regions within each image, which were then spatially aligned with their corresponding fluorescence images to enable extraction of fluorescence measurements from detected bacterial regions while excluding background signal.

Segmentation was evaluated against 222 manually annotated fields of view. The autoencoder achieved a median Dice coefficient of 0.6583 and Intersection-over-Union (IoU) of 0.4907 (standard metrics for quantifying segmentation accuracy), with structural similarity (SSIM) of 0.9910 confirming robust preservation of background and structural integrity. Per-dye median IoU ranged from 0.4557 (DiSC3[5]) to 0.5204 (SYTO 13). Because individual bacterial cells occupy only 10–30 pixels within a 2048 × 1536 image, a single-pixel variance around the cell boundary can shift the IoU score by 15–25%. At this resolution, a median Dice coefficient of 0.66 corresponds to a cellular overlap of over 80%, indicating strong segmentation performance.

In the context of automated cell segmentation, these values indicate a highly robust pipeline with high detection accuracy and low false-positive rates, making it suitable for downstream quantitative analysis.

Morphology validation

Cell morphology was characterised using the axis ratio of each segmented object, defined as the major axis (the longest dimension of the cell) divided by the minor axis (the smallest dimension of the cell). Rod-shaped bacteria and cocci could be differentiated based on the axis ratio with rod-shaped bacteria producing higher axis ratios and cocci yielding ratios closer to one.

As shown in Figure 4, the measured axis ratios form distinct clusters corresponding to cocci and rod morphologies. Rather than hard-thresholding these measurements into discrete morphological bins (which would discard continuous geometric variance and propagate classification errors), the raw continuous geometric descriptors were fed directly into the downstream classification models.

This preserves the complete morphological spectrum of each segmented isolate, enabling the algorithms to leverage subtle, species-specific geometric signatures (such as rod aspect ratio or coccus diameter) alongside spectral data.

Establishing a Unique Multi-Parametric Signature for Uropathogens

Once the uneven illumination and low-frequency imaging artefacts were removed using background correction, histograms were generated for every fluorescence channel and every cell region using the number of pixels falling within each predetermined intensity range.

A Multi-Parametric Signature (MPS) (Figure 5) was then generated by aggregating the cellular morphology metrics – cell shape and size derived from axis analysis of segmented regions – with the fluorescence histograms into a single high-dimensional feature vector. These vectors combined spectral data from all four dye channels (DiSC3(5), SYBR Green I, SYTO 13 and FM 4-64) with cellular morphology metrics, forming a unique biometric signature for each bacterial cell.

As shown in Figure 6, integrating morphological and fluorescence data generates distinct Multi-Parametric Signatures. These distinct patterns enable a clear visual separation of each bacterial species that is used as a reference by the classifier explained below to generate accuracy data.

Classification Performance: Per-species Results and Accuracy

The Histogram Gradient Boosting (HGB) classifier was trained on a dataset of 34,184 images spanning over 191 strains, with the training matrix constructed from component image feature vectors and divided into training and test sets at a 4:1 ratio to ensure balanced representation.

To evaluate the diagnostic value of integrating information across multiple fields of view, we grouped fields of view drawn from the held-out test partition (testing data), at 10 fields of view (FOV) per chamber. For each chamber the per-field class-probability vectors were averaged and a consensus label assigned.

Consensus accuracy reached 99.3% at 10-FOV across all 20 bacterial species (Supplementary Table S5).

This demonstrates that the Multi-Parametric Signatures generated from the four-dye fluorescence panel and morphological features, combined with independent measurements across 10-FOVs, provide sufficient discrimination to distinguish closely related species and a very strong basis for real-world clinical validation.

Classification Performance: Algorithm Comparison

The performance hierarchy across three algorithmic scenarios, Decision Tree, Random Forest and Histogram Gradient Boosting, is consistent with known machine learning theory. The HGB classifier

outperformed both the Decision Tree and Random Forest baselines, achieving near-perfect species-level identification (Figure 7). The histogram binning approach provided two key advantages: faster processing by reducing the number of calculations required during training, and better generalisation by smoothing out minor variations in the fluorescence data. This resulted in a more robust model that performed consistently when identifying held-out records (testing data).

Assay Workflow Summary

The complete assay workflow for bacterial species identification is shown in Figure 8. The pipeline begins with the capture of fluorescent images for each dye, alongside transillumination images of the same sample, providing the foundational optical data.

The geometric morphology data and fluorescence histograms are then combined to generate a unique Multi-Parametric Signature (MPS) for each bacterial cell. Final species identification is achieved by inputting the derived MPS into a classification model driven by a Histogram Gradient Boosting algorithm and comparing against reference signatures.

Across all 191 uropathogenic isolates representing 20 urine-associated bacterial species, the workflow achieved an accuracy of 99.3% with misidentification only observed between some closely related species (Supplementary Tables S3-6).

While these processes are currently separated during development, the finalised system will achieve bacterial species identification within 15 minutes of sample input.

Discussion

This study presents the development and evaluation of a novel multiplexed fluorescence microscopy method for the rapid, culture-free, species-level identification of bacterial uropathogens directly from urine. The method achieves 99.3% species-level accuracy across 20 uropathogenic bacterial species covering both, common community-acquired and nosocomial uropathogens. In this controlled study, the histogram gradient boosting classifier demonstrated a near-perfect ability to distinguish between the 20 target uropathogens using the provided dataset, providing a strong basis for real-world clinical validation. To our knowledge, this is the first demonstration of 99.3% accuracy across a bacterial panel of this breadth, achieved using a method capable of replicating the same in a 15-minute analytical window in a commercial system, using a culture-free approach directly applicable to urine samples.

This assay identifies bacterial species by combining cellular morphology and fluorescence data. The fluorescence aspect uses the differential affinity of four fluorescent dyes for distinct bacterial cellular structures to generate species-specific data. This includes DiSC3(5), SYBR Green I, SYTO 13 and FM 4–64. DiSC3(5) is a membrane-permeable cationic fluorescent dye that accumulates inside polarised, viable bacterial membranes [68,69]. SYBR Green I and SYTO 13 are nucleic acid stains. While SYBR Green I

is highly selective for double-stranded DNA [70,71], SYTO 13 is a non-selective stain that binds both DNA and RNA with comparable affinity [72]. FM 4–64 is a lipophilic compound that binds to the outer lipid leaflet of the cytoplasmic membrane, fluorescing intensely to show cellular boundaries [73,74]. The spectral profile of each dye varies subtly across genera and species, and the combination of four different dyes makes the difference more evident. The morphological component is comprised of cell geometry providing an independent metric that complements the fluorescence data. The combination of cellular morphology and fluorescence data provides the machine learning classifier with a richer and more discriminating representation than either component alone. Feeding this complete Multi-Parametric Signature into the machine learning model results in high identification accuracy.

The diagnostic landscape for rapid bacterial identification in UTI is characterised by a continuous trade-off between breadth of species panel, speed, and accuracy. No existing commercially available rapid identification platform operates across a 20 species panel with species-level accuracy and a ~ 15-minute time-to-result directly from clinical urine at point-of-care.

Our method offers several significant advantages over the current gold standard, the Matrix-Assisted Laser Desorption/Ionization-Time of Flight (MALDI-TOF) mass spectrometry method. While it is highly accurate and covers a larger panel of species than our method, MALDI-TOF requires prior culture growth, is directed towards centralised laboratory settings and cannot process clinical urine directly. The method described in this article operates directly from urine, requires no culture step and is designed for point-of-care implementation.

The performance hierarchy observed across the three algorithmic scenarios: Decision Tree, Random Forest, and Histogram Gradient Boosting at 10-FOV, is consistent with known machine learning theory. When handling high-dimensional, continuous feature spaces (such as multi-spectral fluorescence histograms), gradient boosting frameworks with integrated histogram binning offer well-documented computational and predictive advantages over their counterparts[75,76].

The finding that the HGB classifier, paired with multi-FOV consensus voting, achieves near-perfect species-level identification (99.3% accuracy on holdout data) highlights the power of the Multi-Parametric Signatures generated by the assay.

The clinical implications of achieving accurate, rapid species-level identification at the point of care are substantial. The ability to identify the causative organism within 15 minutes of sample receipt, before the patient leaves the consulting room, would significantly benefit the decision making for UTI which is currently dictated by empirical prescribing. According to United States Food and Drug Administration decision summaries for 510(k)-cleared AST diagnostic systems, organism identification is required for AST result interpretation and reporting[77,78]. The technology described herein directly enables this principle by delivering organism-specific identification at the point of prescribing, enabling downstream AST.

The current identification assay is designed to function as a core module within a broader point-of-care diagnostic system for uncomplicated urinary tract infections. This envisaged system aims to combine bacterial enumeration, identification and AST into a single analytical workflow, utilising one disposable cartridge per patient sample. Therefore, the assay's compatibility with these downstream processes is a critical consideration. By combining these capabilities, the technology functions as a comprehensive, end-to-end UTI diagnostic solution capable of delivering actionable results in approximately 60 minutes.

Several important limitations of the current study must be acknowledged. First, all experiments were conducted using contrived samples i.e., known uropathogenic isolates grown to controlled concentrations (~ 1 x 10^7 CFU/mL) in pooled human urine, rather than clinical urine specimens. The performance of the assay with primary, unprocessed clinical urine samples, which may contain variable bacterial loads (as low as 1 x 10^5 CFU/mL), white blood cells, epithelial cells, commensal flora and diverse concentrations of interfering substances (pH, ionic strength, metabolites), remains to be studied. Second, the study was conducted with a defined panel of 191 strains across 20 species, representing a relatively limited set of strains (up to 10 strains per species) tested compared to the diversity encountered in clinical practice. Expansion of the training and validation dataset to include a larger and more diverse strain collection will be required to fully characterise assay robustness.

Third, the transition from the current benchtop microscope format (EVOS M7000 with glass slides) to a miniaturised, automated cartridge-based platform for true point-of-care deployment introduces additional challenges and such prototypes are currently under assessment. Future work will focus on translating the assay to the Innotive Diagnostics point-of-care system, evaluation with primary clinical specimens in a prospective clinical environment with the integration of enumeration and AST to the same workflow.

Conclusion

This study has successfully developed and evaluated a novel, multiplexed fluorescence microscopy-based diagnostic assay that provides accurate, species-level identification of 20 common uropathogens directly from urine with 99.3% accuracy. The method is designed for integration into an automated platform, aiming to deliver results within around 15 minutes of sample input and be combined with enumeration and antimicrobial susceptibility testing (AST). By generating a Multi-Parametric Signature from synergistic morphological and fluorescence data, and using a Histogram Gradient Boosting classifier, this culture-free method overcomes the critical limitations of both traditional urine culture and existing rapid diagnostic technologies. This culture-free diagnostic technology enables a critical clinical shift from delayed, empirical prescribing to immediate, targeted therapy. By providing clinically actionable species-level information at the point of care, this platform may improve patient outcomes, reduce healthcare costs, support antimicrobial stewardship programmes, and serve as a powerful new tool in the global effort to combat antimicrobial resistance.

Declarations

Data availability

The per-species classification performance data supporting the findings of this study are provided in Supplementary Tables S3-S6. The underlying raw image dataset (34,184 transillumination and fluorescence images) and the derived feature matrices are not publicly available because they constitute commercially sensitive information relating to a diagnostic technology under active development and the subject of pending patent applications (European (EP) Patent Application No: 26170637.8 and U.S. Patent Application No. US20250052744A1). De-identified subsets of these data are available for non-commercial academic verification from the corresponding author. Requests will be reviewed by Innotive Diagnostics Ltd. and answered within 30 days. The access is conditional on a data transfer agreement and data may not be used for commercial purposes or redistributed. The custom code used for image segmentation, feature extraction and classification is proprietary to Innotive Diagnostics Ltd and is not publicly available, as it forms part of a commercial diagnostic system subject to pending patent applications. The algorithms and processing steps are described in full in the Methods section.

Acknowledgements

The authors wish to thank the Innotive Diagnostics staff for their support during this study, namely George Yates and Iris Welsh Price for their support in conducting the experiments, Callum Fraser and Alexander Hellier for their work with the software team, and Dr David Pearce for providing his feedback on the article. The authors thank HCA Healthcare UK Laboratories (London, UK), The Newcastle upon Tyne Hospitals NHS Foundation Trust (Newcastle upon Tyne, UK), and the Culture Collection University of Gothenburg (Göteborg, Sweden) for providing uropathogenic isolates.

Funding

This study was completely funded by Innotive Diagnostics Ltd. No external or grant funding was received for this study.

Author contribution statement

A.D.S. conceived the experiments; S.J. conceived the initial idea; M.V.J. managed the project; D.N. optimised and developed aspects of the experimental protocol and conducted the initial experiments; K.J. and A.B. contributed to experimental work and data collection; A.S., J.R. and D.H. analysed the results. A.D.S., M.V.J., K.J., A.S., D.H., J.R. and S.J. wrote the manuscript. All authors reviewed and approved the final manuscript.

Competing interest statement

This study was funded by Innotive Diagnostics. All authors are employees of Innotive Diagnostics. The technology described in this paper is the subject of two patent applications filed by Innotive Diagnostics Limited (European (EP) Patent Application No: 26170637.8 and U.S. Patent Application No. US20250052744A1).

Ethics declaration

This study did not involve human participants, human tissue or identifiable personal data, and ethical approval was therefore not required. No human samples were received by the authors at any stage, only bacterial isolates, were transferred. No patient-identifiable information, clinical metadata or linked records were provided, and the isolates cannot be traced to individual patients by the authors. The pooled human urine used as a growth matrix was obtained commercially (Drug-Free Pooled Human Urine, 2B Scientific, UK) and was supplied fully anonymised.

References

1. Naghavi, M. et al. Global burden of bacterial antimicrobial resistance 1990–2021: a systematic analysis with forecasts to 2050. *Lancet* **404**, 1199–1226 (2024).
2. O'Neill, J. *Tackling Drug-Resistant Infections Globally: Final Report And Recommendations*. 84 (2016).
3. WHO. Antimicrobial resistance. (2023). https://www.who.int/news-room/fact-sheets/detail/antimicrobial-resistance
4. Andersson, D. I. & Hughes, D. Antibiotic resistance and its cost: is it possible to reverse resistance? *Nat. Rev. Microbiol.* **8**, 260–271 (2010).
5. Gelband, H. & Laxminarayan, R. Tackling antimicrobial resistance at global and local scales. *Trends Microbiol.* **23**, 524–526 (2015).
6. Mendelson, M., Balasegaram, M., Jinks, T., Pulcini, C. & Sharland, M. Antibiotic resistance has a language problem. *Nature* **545**, 23–25 (2017).
7. Roca, I. et al. The global threat of antimicrobial resistance: science for intervention. *New. Microbes New. Infect.* **6**, 22–29 (2015).
8. Bryce, A. et al. Global prevalence of antibiotic resistance in paediatric urinary tract infections caused by *Escherichia coli* and association with routine use of antibiotics in primary care: systematic review and meta-analysis. *BMJ* i939 (2016). 10.1136/bmj.i939
9. Cek, M. et al. Healthcare-associated urinary tract infections in hospitalized urological patients—a global perspective: results from the GPIU studies 2003–2010. *World J. Urol.* **32**, 1587–1594 (2014).
10. Tandogdu, Z. et al. Urosepsis 30-day mortality, morbidity, and their risk factors: SERPENS study, a prospective, observational multi-center study. *World J. Urol.* **42**, 314 (2024).
11. Kerremans, J. J. et al. Rapid identification and antimicrobial susceptibility testing reduce antibiotic use and accelerate pathogen-directed antibiotic use. *J. Antimicrob. Chemother.* **61**, 428–435 (2007).
12. Van Belkum, A. et al. Innovative and rapid antimicrobial susceptibility testing systems. *Nat. Rev. Microbiol.* **18**, 299–311 (2020).
13. Yang, X. et al. Disease burden and long-term trends of urinary tract infections: A worldwide report. *Front. Public. Health*. **10**, 888205 (2022).

14. Goebel, M. C., Trautner, B. W. & Grigoryan, L. The Five Ds of Outpatient Antibiotic Stewardship for Urinary Tract Infections. *Clin. Microbiol. Rev.* **34**, e00003–20 (2021).
15. Clark, A. W. et al. Rural–urban differences in antibiotic prescribing for uncomplicated urinary tract infection. *Infect. Control Hosp. Epidemiol.* **42**, 1437–1444 (2021).
16. Murray, K., Shimabukuro, J., Khalfay, N. & Chiang, J. N. Lenore Ackerman, A. Antibiotic Overprescription for Urinary Tract Infections Is Associated With Poor Diagnostic Stewardship and Low Adherence to Guidelines. *Neurourol. Urodyn.* **44**, 382–389 (2025).
17. Ciaccio, L. et al. Trends in urine sampling rates of general practice patients with suspected lower urinary tract infections in England, 2015–2022: a population-based study. *BMJ Open.* **14**, e084485 (2024).
18. Foxman, B. The epidemiology of urinary tract infection. *Nat. Rev. Urol.* **7**, 653–660 (2010).
19. Esteve-Palau, E. et al. Clinical and economic impact of urinary tract infections caused by ESBL-producing Escherichia coli requiring hospitalization: A matched cohort study. *J. Infect.* **71**, 667–674 (2015).
20. Flores-Mireles, A. L., Walker, J. N., Caparon, M. & Hultgren, S. J. Urinary tract infections: epidemiology, mechanisms of infection and treatment options. *Nat. Rev. Microbiol.* **13**, 269–284 (2015).
21. Medina, M. & Castillo-Pino, E. An introduction to the epidemiology and burden of urinary tract infections. *Ther. Adv. Urol.* **11**, 1756287219832172 (2019).
22. Gbinigie, O. A., Ordóñez-Mena, J. M., Fanshawe, T. R., Plüddemann, A. & Heneghan, C. Diagnostic value of symptoms and signs for identifying urinary tract infection in older adult outpatients: Systematic review and meta-analysis. *J. Infect.* **77**, 379–390 (2018).
23. Carreno, J. J. et al. Nationwide, Cohort Study to Assess Incidence, Outcomes, and Costs Associated with Complicated Urinary Tract Infection. *Open. Forum Infect. Dis.* **ofz446** 10.1093/ofid/ofz446 (2019). Longitudinal.
24. Broughton, E., Colosia, A., Bektas, M., Kuper, K. & Kotb, R. Assessing the economic burden of complicated urinary tract infection: A systematic literature review. *Eur. J. Health Econ.* https://doi.org/10.1007/s10198-025-01846-8 (2025).
25. Zilberberg, M. D., Nathanson, B. H., Sulham, K. & Shorr, A. F. Descriptive epidemiology and outcomes of emergency department visits with complicated urinary tract infections in the United States, 2016–2018. *JACEP Open.* **3**, e12694 (2022).
26. Grey, B., Upton, M. & Joshi, L. T. Urinary tract infections: a review of the current diagnostics landscape. *J Med. Microbiol* **72**, (2023).
27. Zhu, N. J. et al. Economic Burden of Community-Acquired Antibiotic-Resistant Urinary Tract Infections: Systematic Review and Meta-Analysis. *JMIR Public. Health Surveill*. **10**, e53828–e53828 (2024).
28. Irvine, A. et al. The Importance of Diagnostics in the Treatment of Urinary Tract Infections in the United Kingdom. *Res. Rep. Urol.* **16**, 327–335 (2024).

29. Schmiemann, G., Kniehl, E., Gebhardt, K., Matejczyk, M. M. & Hummers-Pradier, E. The Diagnosis of Urinary Tract Infection. *Dtsch. Ärztebl Int.* https://doi.org/10.3238/arztebl.2010.0361 (2010).
30. Xu, R., Deebel, N., Casals, R., Dutta, R. & Mirzazadeh, M. A. New Gold Rush: A Review of Current and Developing Diagnostic Tools for Urinary Tract Infections. *Diagnostics* **11**, 479 (2021).
31. Perry, J. D. A Decade of Development of Chromogenic Culture Media for Clinical Microbiology in an Era of Molecular Diagnostics. *Clin. Microbiol. Rev.* **30**, 449–479 (2017).
32. Dudzik, Ł., Krzyżek, P. & Dworniczek, E. A. Review on the Current and Future State of Urinary Tract Infection Diagnostics. *Int. J. Mol. Sci.* **26**, 10847 (2025).
33. Ben-David, D., Cohen, Y., Zohar, I., Maor, Y. & Schwartz, O. The impact of Boric Acid tubes on quantitative urinary bacterial cultures in hospitalized patients. *Eur. J. Clin. Microbiol. Infect. Dis.* **43**, 1639–1644 (2024).
34. LaRocco, M. T. et al. Effectiveness of Preanalytic Practices on Contamination and Diagnostic Accuracy of Urine Cultures: a Laboratory Medicine Best Practices Systematic Review and Meta-analysis. *Clin. Microbiol. Rev.* **29**, 105–147 (2016).
35. Hayward, G. et al. Urine collection devices to reduce contamination in urine samples for diagnosis of uncomplicated UTI: a single-blind randomised controlled trial in primary care. *Br. J. Gen. Pract.* **72**, e225–e233 (2022).
36. Pothoven, R. Management of urinary tract infections in the era of antimicrobial resistance. *Drug Target. Insights*. **17**, 126–137 (2023).
37. WHO. Antimicrobial resistance: global report on surveillance. (2014). https://www.who.int/publications/i/item/9789241564748
38. Devillé, W. L., Yzermans, J. C., van Duijn, N. P. & Bezemer, D. The urine dipstick test useful to rule out infections. A meta-analysis of the accuracy. (2004).
39. Kristensen, L. H. et al. Diagnostic accuracy of dipsticks for urinary tract infections in acutely hospitalised patients: a prospective population-based observational cohort study. *BMJ Evid. -Based Med.* **30**, 36–44 (2025).
40. Wright, O. R. & Safranek, S. Urine Dipstick for Diagnosing Urinary Tract Infection. https://www.aafp.org/afp/2006/0101/p129
41. Almuhanna, H. S. et al. Comparison Between Urine Dipstick and Microscopic Examination Urinalysis With Urine Culture to Evaluate the Sensitivity and Specificity for Each in Diagnosing Urinary Tract Infection in Qassim Region, Saudi Arabia. *Cureus* 16, e59069.
42. Maina, J. et al. Evaluation of the diagnostic performance of the urine dipstick test for the detection of urinary tract infections in patients treated in Kenyan hospitals. *Access. Microbiol.* **5**, acmi000483v3 (2023).
43. Moragas, A., Monfà, R., García-Sangenís, A. & Llor, C. Accuracy of leukocyte esterase and nitrite tests for diagnosing bacteriuria in older adults: A systematic review and meta-analysis. *Clin. Microbiol. Infect. Off Publ Eur. Soc. Clin. Microbiol. Infect. Dis.* **S1198-743X** (25), 00425–00422. 10.1016/j.cmi.2025.08.027 (2025).

44. Abubakar, M. U., Abdullahi, S. H., Xiong, M. & He, B. Label-free phenotypic antimicrobial susceptibility testing on microfluidic platforms: a review of advances and translation. *Microchim Acta*. **192**, 808 (2025).
45. Bermudez, T., Schmitz, J. E., Boswell, M. & Humphries, R. Novel technologies for the diagnosis of urinary tract infections. *J. Clin. Microbiol.* **63**, e00306–e00324 (2025).
46. Rattin, J., Boswell, M. & Rhoads, D. Emerging technologies for rapid phenotypic antimicrobial susceptibility testing of clinical isolates of bacteria. *J. Clin. Microbiol.* **63**, e00674–e00625 (2025).
47. Reszetnik, G. et al. Next-generation rapid phenotypic antimicrobial susceptibility testing. *Nat. Commun.* **15**, 9719 (2024).
48. Davaro, E., Tomaras, A. P., Chamberland, R. R. & Isbell, T. S. Evaluation of a Novel Light Scattering Methodology for the Detection of Pathogenic Bacteria in Urine. *J. Appl. Lab. Med.* **5**, 370–376 (2020).
49. Montgomery, S. et al. Prospective Evaluation of Light Scatter Technology Paired with Matrix-Assisted Laser Desorption Ionization – Time of Flight Mass Spectrometry for Rapid Diagnosis of Urinary Tract Infections. *J. Clin. Microbiol.* **55**, 1802–1811 (2017).
50. Boon, H. A., De Burghgraeve, T., Verbakel, J. Y. & Van Den Bruel, A. Point-of-care tests for pediatric urinary tract infections in general practice: a diagnostic accuracy study. *Fam Pract.* **39**, 616–622 (2022).
51. Teppa, R. J. & Roberts, J. M. The Uriscreen Test to Detect Significant A symptomatic Bacteriuria During Pregnancy. *J. Soc. Gynecol. Investig*. **12**, 50–53 (2005).
52. Ganguly, A. et al. A label-free, rapid, non-culture based biosensing platform for urinary tract infection diagnosis and management. *J Urol* **209**, (2023).
53. Iseri, E., Nilsson, S., Van Belkum, A., Van Der Wijngaart, W. & Özenci, V. Performance of an innovative culture-based digital dipstick for detection of bacteriuria. *Microbiol. Spectr.* **12**, e03613–e03623 (2024).
54. Alonso-Tarrés, C. et al. Bacteriuria and phenotypic antimicrobial susceptibility testing in 45 min by point-of-care Sysmex PA-100 System: first clinical evaluation. *Eur. J. Clin. Microbiol. Infect. Dis.* **43**, 1533–1543 (2024).
55. Elsisi, G. H., Zaky, H. S. & Polo, J. M. Budget impact analysis on the use of Sysmex PA-100 AST system as a point of care for uncomplicated urinary tract infections detection and treatment in Spanish females. *J. Med. Econ.* **27**, 1434–1443 (2024).
56. Al-Adhami, M., Tilahun, D., Rao, G., Gurramkonda, C. & Kostov, Y. Rapid detection of microbial contamination using a microfluidic device. in Biosensors and Biodetection: Methods and Protocols Volume 1: Optical-Based Detectors 287–299 (Springer, (2017).
57. Bock, L. J. et al. Rapid impedance-based Antimicrobial Susceptibility Testing (iFAST) of Enterobacterales in urinary tract infections. *J. Infect.* **91**, 106549 (2025).
58. Burg, L. et al. Rapid pathogen identification and phenotypic antimicrobial susceptibility directly from urine specimens. *Sci. Rep.* **12**, 18315 (2022).

59. Chan, C. C. Y. et al. Metabolomics strategy for diagnosing urinary tract infections. *Nat. Commun.* **16**, 2658 (2025).
60. Domingo-Roca, R. et al. Rapid assessment of antibiotic susceptibility using a fully 3D-printed impedance-based biosensor. *Biosens. Bioelectron. X*. **13**, 100308 (2023).
61. Jindal, S., Thampy, H., Day, P. J. R. & Kell, D. B. Very rapid flow cytometric assessment of antimicrobial susceptibility during the apparent lag phase of microbial (re)growth. *Microbiology* **165**, 439–454 (2019).
62. Spencer, D. C. et al. A fast impedance-based antimicrobial susceptibility test. *Nat. Commun.* **11**, 5328 (2020).
63. Stratford, J. P. et al. Electrically induced bacterial membrane-potential dynamics correspond to cellular proliferation capacity. *Proc. Natl. Acad. Sci.* 116, 9552–9557 (2019).
64. Tarlton, N. J. et al. A Dual Enzyme-Based Biochemical Test Rapidly Detects Third-Generation Cephalosporin-Resistant CTX-M-Producing Uropathogens in Clinical Urine Samples. *Microb. Drug Resist.* **27**, 450–461 (2021).
65. Diggle, J. et al. Lodestar DX, an evaluation: loop-mediated isothermal amplification (LAMP) for the diagnosis of urinary tract infection in symptomatic adult females. *JAC-Antimicrob Resist.* **6**, dlae148 (2024).
66. Pattern Bioscience. Our Technology. *Pattern Bioscience* (2026). https://pattern.bio/our-tech/
67. Vendeville, J. B. et al. Fast Identification and Quantification of Uropathogenic *E. coli* through Cluster Analysis. *ACS Biomater. Sci. Eng.* **8**, 242–252 (2022).
68. Te Winkel, J. D., Gray, D. A., Seistrup, K. H., Hamoen, L. W. & Strahl, H. Analysis of Antimicrobial-Triggered Membrane Depolarization Using Voltage Sensitive Dyes. *Front Cell. Dev. Biol* **4**, (2016).
69. Waggoner, A. Optical probes of membrane potential. *J. Membr. Biol.* **27**, 317–334 (1976).
70. Nescerecka, A., Hammes, F. & Juhna, T. A pipeline for developing and testing staining protocols for flow cytometry, demonstrated with SYBR Green I and propidium iodide viability staining. *J. Microbiol. Methods*. **131**, 172–180 (2016).
71. Prest, E. I., Hammes, F., Kötzsch, S., Van Loosdrecht, M. C. M. & Vrouwenvelder, J. S. Monitoring microbiological changes in drinking water systems using a fast and reproducible flow cytometric method. *Water Res.* **47**, 7131–7142 (2013).
72. Mason, D. J., Shanmuganathan, S., Mortimer, F. C. & Gant, V. A. A Fluorescent Gram Stain for Flow Cytometry and Epifluorescence Microscopy. *Appl. Environ. Microbiol.* **64**, 2681–2685 (1998).
73. Muchová, K., Wilkinson, A. J. & Barák, I. Changes of lipid domains in Bacillus subtilis cells with disrupted cell wall peptidoglycan. *Fems Microbiol. Lett.* **325**, 92–98 (2011).
74. Pogliano, J. et al. A vital stain for studying membrane dynamics in bacteria: a novel mechanism controlling septation during *Bacillus subtilis* sporulation. *Mol. Microbiol.* **31**, 1149–1159 (1999).
75. Friedman, J. H. Greedy Function Approximation: A Gradient Boosting Machine. *Ann. Stat.* **29**, 1189–1232 (2001).

76. Ke, G. et al. LightGBM: A Highly Efficient Gradient Boosting Decision Tree.
77. Food, U. S. & Drug Administration. and. *510(k) Substantial Equivalence Determination Decision Summary for K221688*. (2023). https://www.accessdata.fda.gov/cdrh_docs/reviews/K221688.pdf
78. Food, U. S. & Drug Administration. and. *510(k) Substantial Equivalence Determination Decision Summary for K230675*. (2024). https://www.accessdata.fda.gov/cdrh_docs/reviews/K230675.pdf

Figures

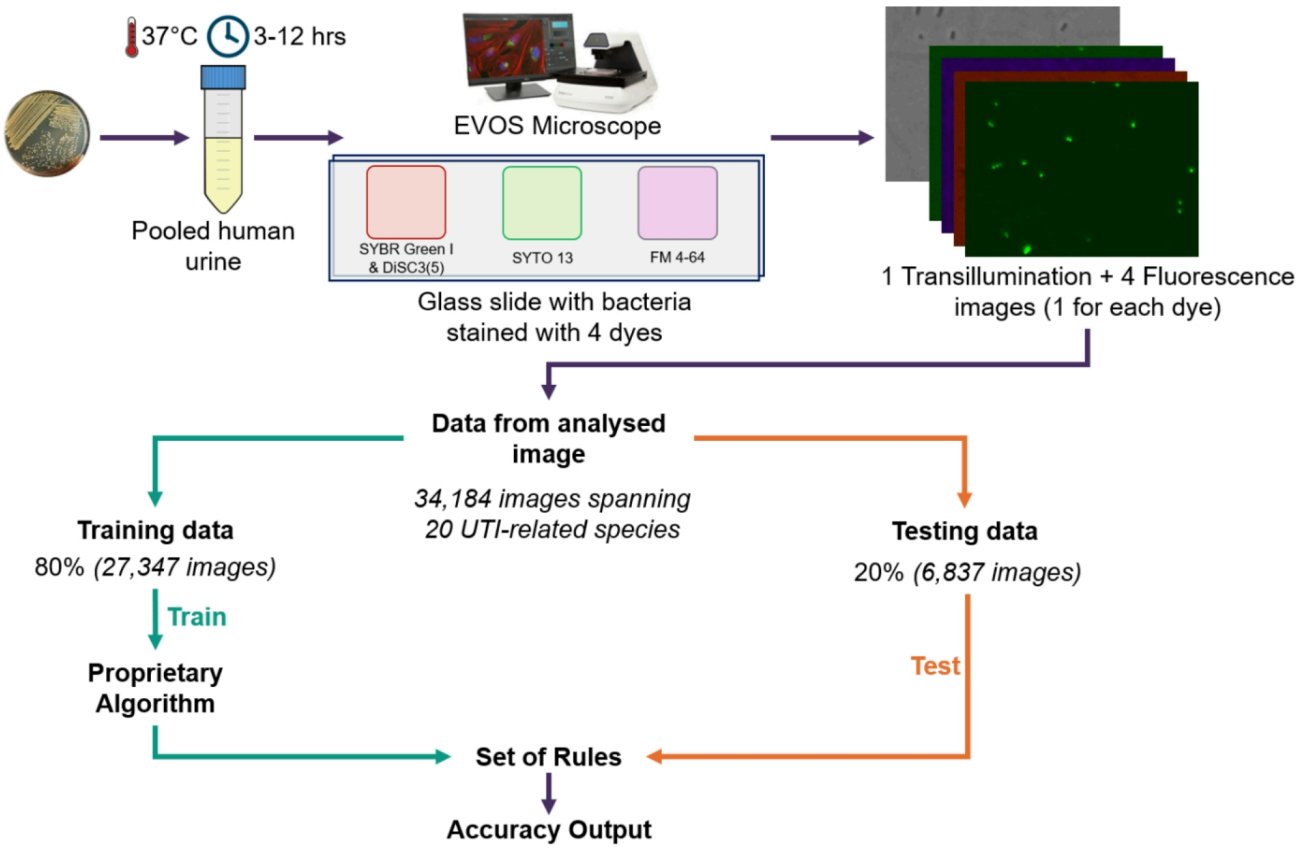


Figure 1

Schematic overview of the sample processing and machine learning workflow. Urine samples spiked with bacterial strains were incubated and subsequently stained using a four-dye multiplex panel comprising SYBR Green I, SYTO 13, DiSC3(5) and FM 4-64. For each sample, an EVOS microscope acquired transillumination and corresponding fluorescence images for each dye. Across the 20 UTI-related species, this resulted in an initial dataset of 34,184 images. The extracted multi-parametric data was randomly divided, with 80% (27,347 images) allocated to train the proprietary predictive algorithm, generating a robust set of classification rules. The remaining 20% (6,837 images) was reserved as a blind testing dataset to evaluate the algorithm's accuracy output.

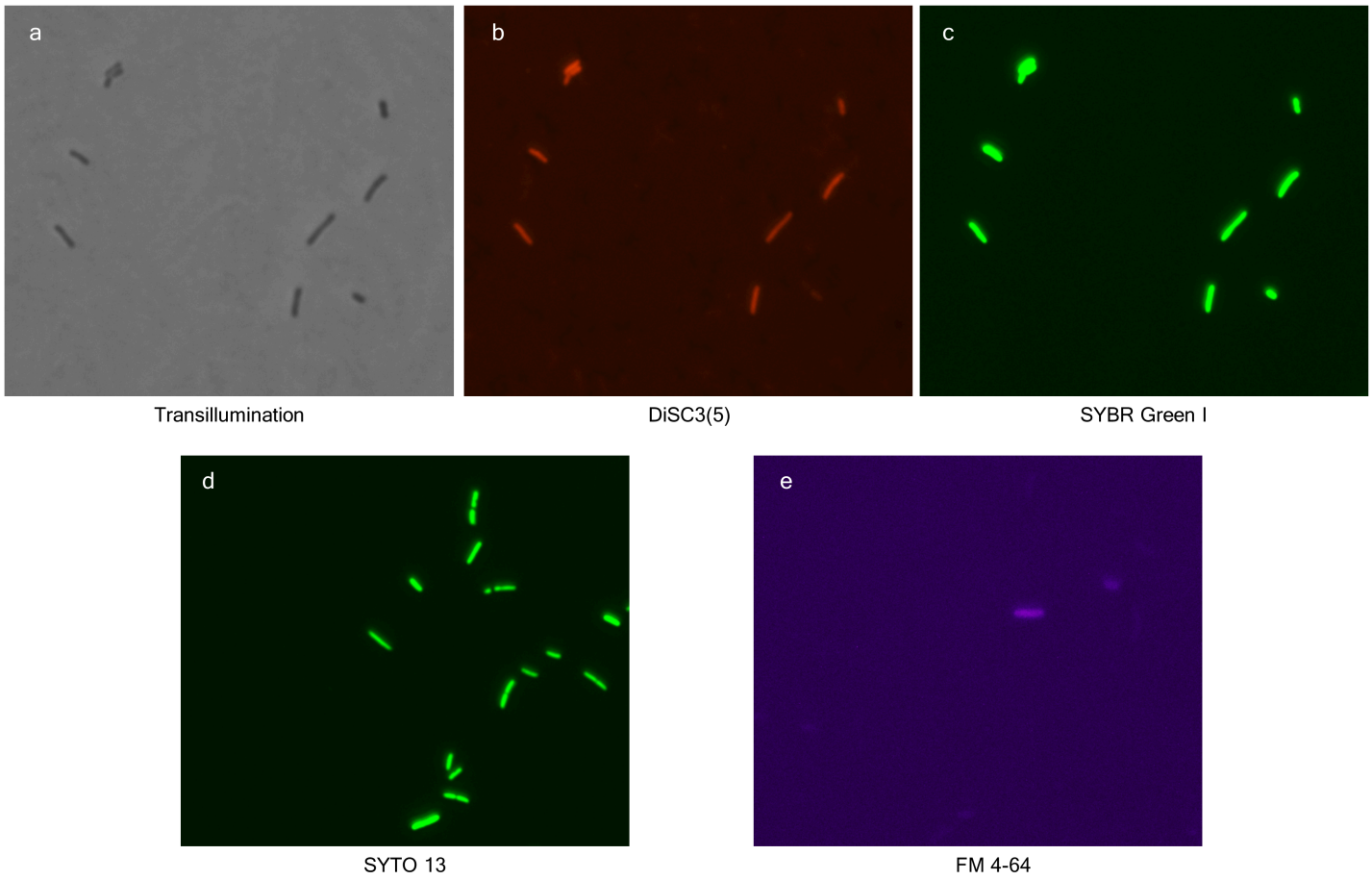


Figure 2

Representative multi-channel optical images of a uropathogenic *E. coli* isolate. (a) Transilluminationimage used for geometric analysis and cellular segmentation. **(b-e)** Individual fluorescent images for four different dyes staining the isolate. The corresponding fluorescence channels are **(b)** DiSC3(5), **(c)** SYBR Green I, **(d)** SYTO 13 and **(e)** FM 4-64. The transilluminationimage displayed in **(a)** corresponds to the same specimen and location as that of the DiSC3(5) and SYBR Green I captures. Transilluminationreference images for the SYTO 13 and FM 4-64 specimensare not shown.

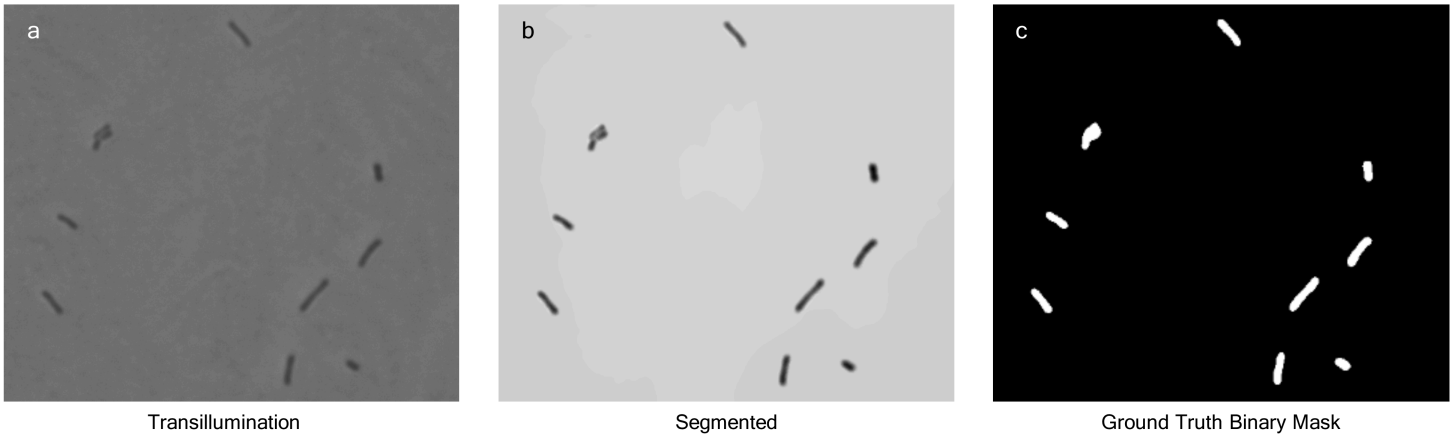


Figure 3

Image preprocessing steps for bacterial analysis of a uropathogenic *E. coli* isolate. The pipeline comprises: **(a)** the raw transillumination image, which undergoes background subtraction to enhance bacterial visibility; **(b)** a convolutional neural network generates a binary segmentation mask identifying cell regions, which serves as **(c)** the manually annotated ground truth for quantitative evaluation. This mask is then spatially aligned with fluorescence images to ensure accurate correspondence between segmentation and fluorescence data.

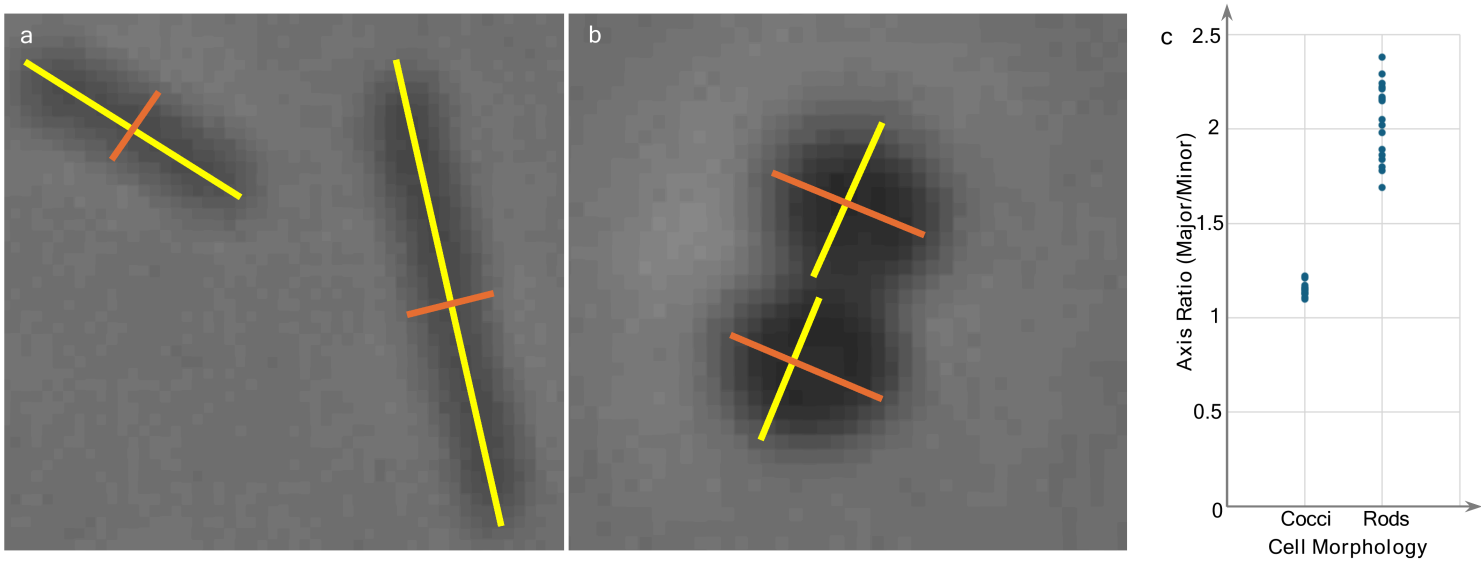


Figure 4

Morphological classification using axis ratio of clinical *E. coli* and *S. saprophyticus* isolates. Cell morphology was characterised by the ratio of major axis length to minor axis length calculated from each segmented object. **(a)**Rod-shaped bacteria (*E. coli*) exhibit a substantially larger major axis than minor axis, producing higher axis ratios; **(b)** cocci (*S. saprophyticus*) possess similar dimensions in both directions, yielding ratios closer to one. **(c)** The measured axis ratios form distinct clusters corresponding to cocci and rod morphologies, enabling automated differentiation between cell types. This geometric descriptor provides a simple and robust method for morphological classification independent of fluorescence intensity or staining characteristics.

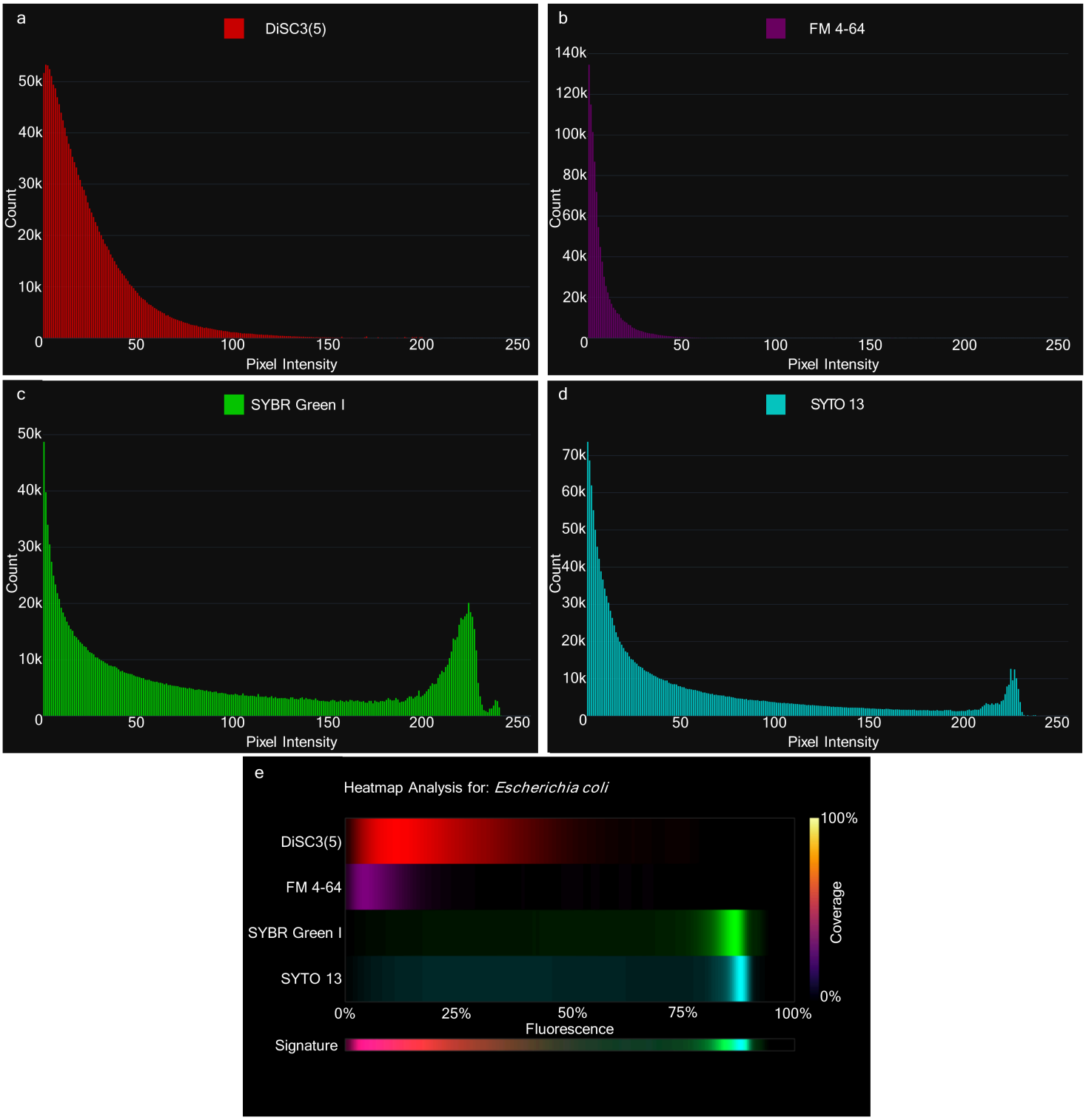


Figure 5

Spectral distribution analysis and Multi-Parametric Signature (MPS) generation. Following background correction to remove uneven illumination and low-frequency imaging artefacts, histograms were computed by counting the number of pixels falling within each predetermined intensity range, producing **(a-d)** a frequency distribution for every fluorescence dye (DiSC3(5), FM 4-64, SYBR Green I and SYTO 13) and every cell region. **(e)** Heatmap analysis for the representative *Escherichia coli* isolate showcasing the

relative fluorescence intensity coverage across each channel. These individual spectral distributions are combined with cellular morphology metrics (cell shape and size derived from major/minor axis analysis) into a single, high-dimensional feature vector, producing a unique Multi-Parametric Signature (bottom bar) for rapid bacterial identification.

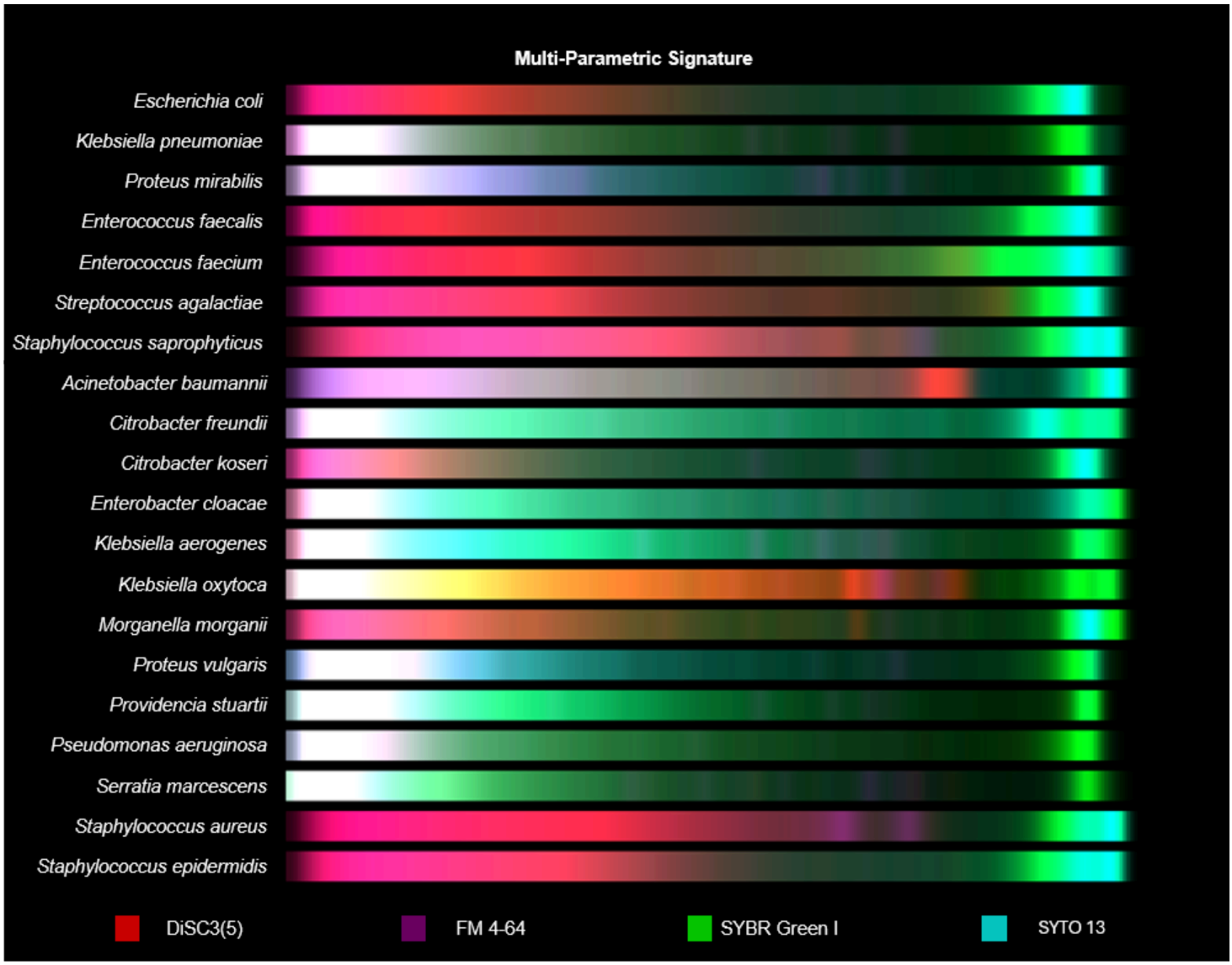


Figure 6

Multi-Parametric Signatures (MPS). Fluorescence intensity histograms rendered as heatmaps reveal distinct spectral profiles across species. Each bacterial species exhibited a characteristic pattern of dye uptake and fluorescence distribution, producing composite species spectra that enabled clear visual differentiation between species. The combination of morphological and fluorescence data provided a richer, more discriminating representation than either component alone; the spectral profile captured differential affinity of dyes for distinct bacterial cellular structures, while morphology provided an independent geometric descriptor.

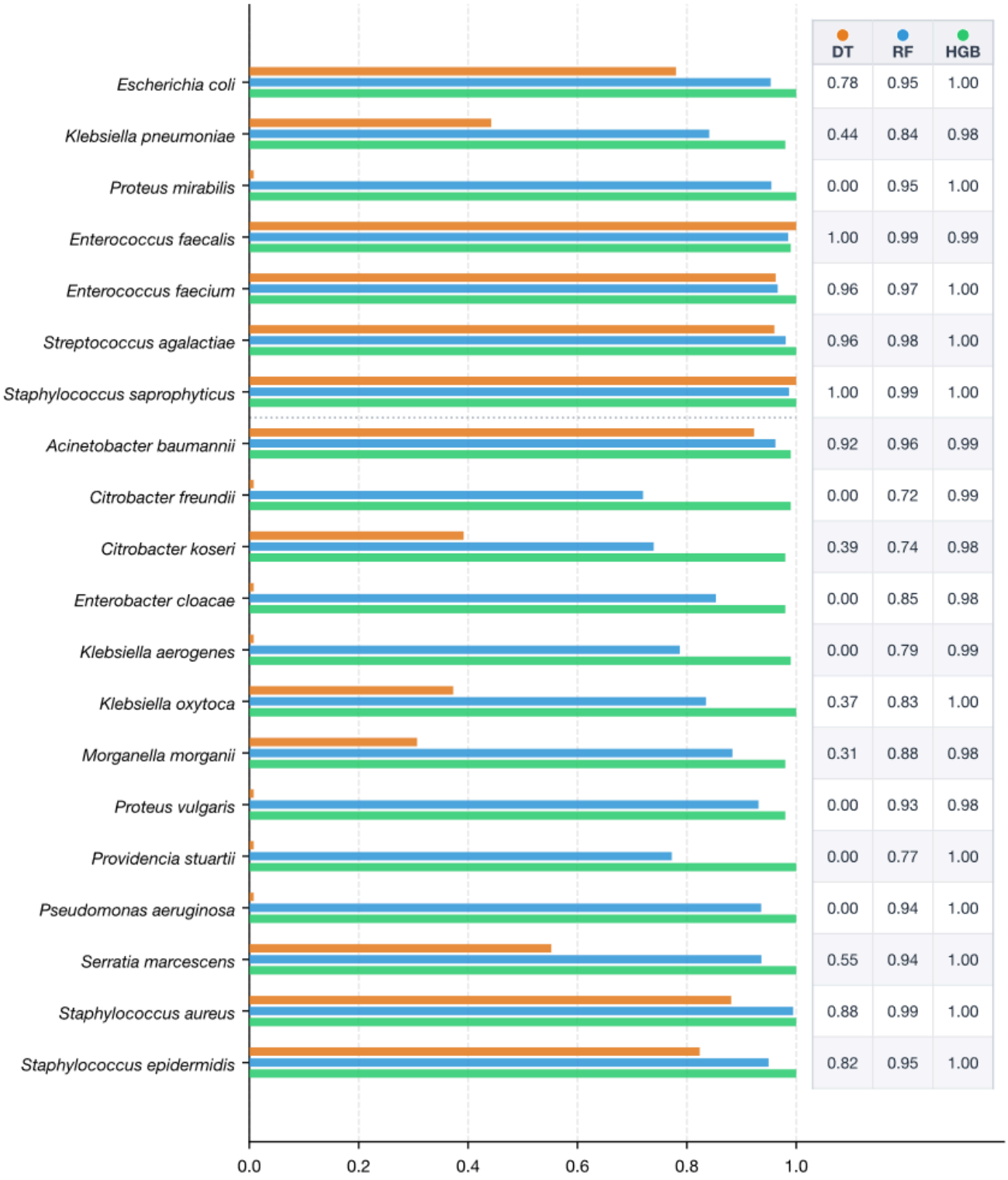


Figure 7

Algorithm comparison: F1-score across bacterial species. The performance hierarchy across three algorithmic scenarios, Decision Tree, Random Forest and Histogram Gradient Boosting (HGB). The HGB consensus models dramatically outperformed the other two scenarios, achieving near-perfect species-level identification (99.3% at 10-FOV). The histogram binning approach of HGB provided faster

processing and better generalisation, which, when paired with multi-FOV consensus, resulted in a highly robust workflow that performed consistently across all 20 target uropathogenic species.

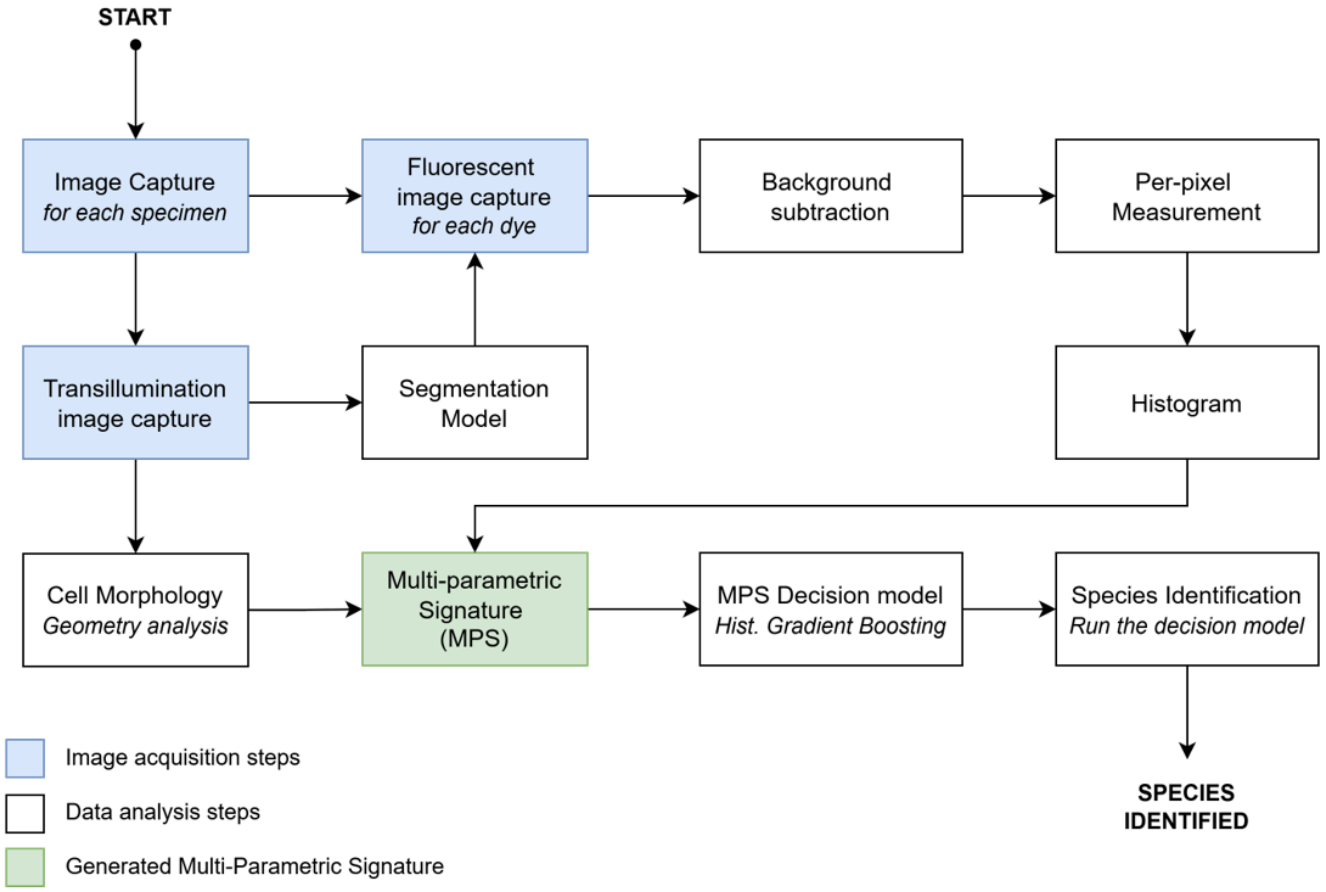


Figure 8

Automated workflow for bacterial species identification. The schematic details the pipeline from initial image capture using fluorescent and transillumination (blue) to the data analysis steps (white). A Multi-Parametric Signature (green) is generated by combining morphological data and fluorescence histograms, which is then processed using a Histogram Gradient Boosting model to identify the species for each sample.

Supplementary Files

This is a list of supplementary files associated with this preprint. Click to download.

- COM027BenchtopBacterialIdentificationJournalArticleSupplemetaryData.docx